Journal of Safety Science and Resilience 4 (2023) 366–379

Contents lists available at ScienceDirect

Journal of Safety Science and Resilience

journal homepage: www.keaipublishing.com/en/journals/journal-of-safety-science-and-resilience/

Underground storage tank blowout analysis: Stability prediction using an artificial neural network

Nhat Tan Duong [a], Van Qui Lai [a], Jim Shiau [b], Rungkhun Banyong [c], Suraparb Keawsawasvong [c,*]

[a] *Faculty of Civil Engineering, Ho Chi Minh City University of Technology (HCMUT), VNU-HCM, Ho Chi Minh City, Vietnam*
[b] *School of Engineering, University of Southern Queensland, Toowoomba 4350, QLD, Australia*
[c] *Research Unit in Sciences and Innovative Technologies for Civil Engineering Infrastructures, Department of Civil Engineering, Thammasat School of Engineering, Thammasat University, Pathumthani 12120, Thailand*

ARTICLE INFO

Keywords:
Blowout
Passive stability
Trapdoor
Stability factors
Limit analysis

ABSTRACT

Most geotechnical stability research is linked to “active” failures, in which soil instability occurs due to soil self-weight and external surcharge applications. In contrast, research on passive failure is not common, as it is predominately caused by external loads that act against the soil self-weight. An earlier active trapdoor stability investigation using the Terzaghi’s three stability factor approach was shown to be a feasible method for evaluating cohesive-frictional soil stability. Therefore, this technical note aims to expand “active” trapdoor research to assess drained circular trapdoor passive stability (blowout condition) in cohesive-frictional soil under axisymmetric conditions. Using numerical finite element limit analysis (FELA) simulations, soil cohesion, surcharge, and soil unit weight effects are considered using three stability factors (F_c, F_s, and F_γ), which are all associated with the cover-depth ratio and soil internal friction angle. Both upper-bound (UB) and lower-bound (LB) results are presented in design charts and tables, and the large dataset is further studied using an artificial neural network (ANN) as a predictive model to produce accurate design equations. The proposed passive trapdoor problem under axisymmetric conditions is significant when considering soil blowout stability owing to faulty underground storage tanks or pipelines with high internal pressures.

1. Introduction

The classical active trapdoor problem has been considered a fundamental geotechnical stability issue since the innovative study by Terzaghi [1]. As the word “active” suggests, active failures are primarily caused by soil self-weight and surface surcharge. Typical active failure problems include lateral earth pressure, and trapdoor, slope, and tunnel-heading stability.

In contrast, passive failures are related to excessive pressure acting opposite to the soil gravity direction. On occasion, they are called blowout or uplift failures, in which the internal pressure is much greater than the soil shear resistance and self-weight. Owing to the growing population and metropolitan infrastructure development expansion, the demand for subterranean sanitary systems such as various underground storage tanks (water, biogas, and fuel storage tanks) has increased dramatically over the past decades. The demand for underground facilities has highlighted soil stability importance, particularly in blowout stability evaluation.

Previous studies on buried anchor uplift capability in soils were conducted through experimentation by Meyerhof and Adams [2], Vesic [3], Meyerhof [4], and Das [5,6]. Vardoulakis et al. [7] conducted a sequence of physical experiments on cohesionless sand and provided analytical conclusions for both passive and active trapdoors. A wedge extending from a particular trapdoor to the ground surface was utilized to illustrate the passive situation. For computational studies, Koutsabeloulis and Griffiths [8] conducted several finite-element analyses on active and passive trapdoors in soils. Using the discontinuity layout optimization method in conjunction with upper-bound (UB) limit analysis, Smith [9] established a computer-based method for calculating the trapdoor load ratio in cohesionless soils. Martin [10] employed both UB and lower-bound (LB) techniques while applying a unique slip line procedure to estimate the genuine collapse load for undrained active and passive trapdoor stability problems. Wang et al. [11] investigated active and passive soil arching techniques for planar trapdoors in cohesive-frictional soils. No surcharge loading was considered, and complex load ratio normalization limited its practicability.

* Corresponding author.
E-mail address: ksurapar@engr.tu.ac.th (S. Keawsawasvong).

https://doi.org/10.1016/j.jnlssr.2023.09.002
Received 16 July 2023; Received in revised form 18 September 2023; Accepted 18 September 2023
Available online 18 October 2023

Shallow foundation load-bearing capacity has frequently been determined using three stability factors and the superposition technique, which are both widely known as Terzaghi's bearing capacity factors [12]. This approach has recently been recognized as an effective method for collapse load estimation and has been applied to various underground stability problems in cohesive-frictional soils [13–15]. The Terzaghi equation was modified to evaluate active failures, as shown in Eq. (1).

$$\sigma_t = -cF_c + \sigma_s F_s + \gamma D F_\gamma \tag{1}$$

In Eq. (1), the minimum support pressure (σ_t) is determined by the mathematical formulation of three stability factors, namely the cohesion factor (F_c), the surcharge factor (F_s), and the unit weight factor (F_γ). The primary design parameters are soil cohesion c, surcharge σ_s, soil unit weight γ, and tunnel diameter D [13]. The negative sign in the first term of Eq. (1) suggests that the cohesive strength works in opposition to the soil surcharge motions and soil unit weight.

It should be emphasized that by removing the negative sign in Eq. (1), a new equation can be created to assess passive failure (blowout/uplift failure). This is shown in Eq. (2).

$$\sigma_t = cF_c + \sigma_s F_s + \gamma D F_\gamma \tag{2}$$

According to Eq. (2), the stability factor can be calculated individually by adjusting certain parameters to zero, except for the parameter of interest. For example, in these calculations, $\gamma = 0$ and $\sigma_s = 0$ values were used to calculate $\sigma_t = cF_c$. The other two stability factors (F_s and F_γ) can be calculated in a similar manner. Further details on the numerical operation are available in Shiau and Al-Asadi [13].

The main objective of this study is to broaden the stability solution for a trustworthy drained circular trapdoor evaluation in cohesive-frictional soil under axisymmetric conditions. The passive trapdoor problem is assumed to represent a soil blowout incident caused by a faulty subterranean storage tank under high internal pressure. Recently developed UB and LB finite element limit analysis (FELA) was employed to produce rigorous solutions for practical use. Using a large FELA result dataset, an artificial neural network (ANN) model was established to produce novel formulae for predicting the three stability factors. This study aims to provide accurate equations for predicting trapdoor blowout stability in cohesive-frictional soils under axisymmetric conditions. Novel formulae can improve working design speed compared with traditional methods, such as modeling or interpolating using a design chart. Practitioners can use novel formulae in MS Excel to immediately perform hundreds of tasks.

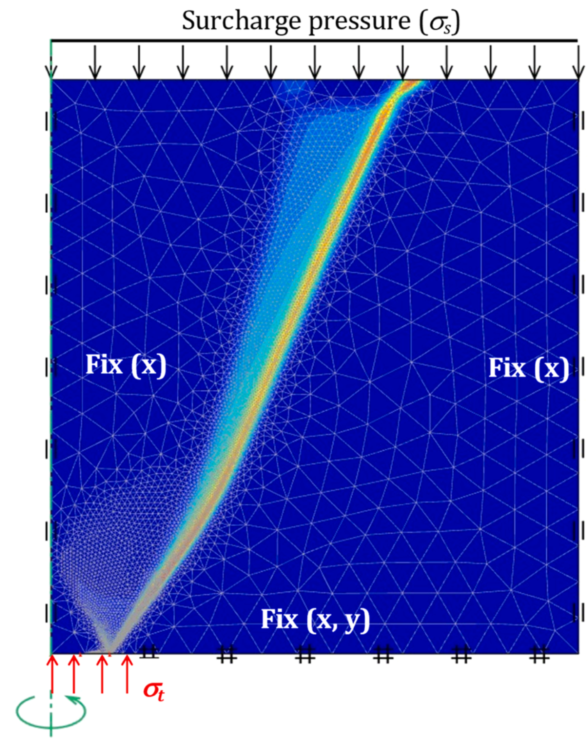

Fig. 2. A numerical model, boundary condition and adaptive mesh for F_γ analysis ($H/D = 3$).

2. Problem statement and three stability factors

The problem definition for passive trapdoors in cohesive-frictional soil under axisymmetric conditions is illustrated in Fig. 1. The trapdoor has a diameter (D) and a cover depth (H) measured from the top surface of the ground with a uniform surface pressure (σ_s). On the trapdoor surface, a uniform uplift pressure (σ_t) was applied vertically in the opposite direction to the soil self-weight and surcharge loading. Three soil properties were used to represent the soil strength profile as the soil mass satisfied the Mohr-Coulomb yield criteria: drained cohesion (c), drained friction angle (ϕ), and soil unit weight (γ). Note that this study proposes a perfectly ideal engineering case, which is a circular trapdoor in cohesive-frictional soil under axisymmetric conditions. This

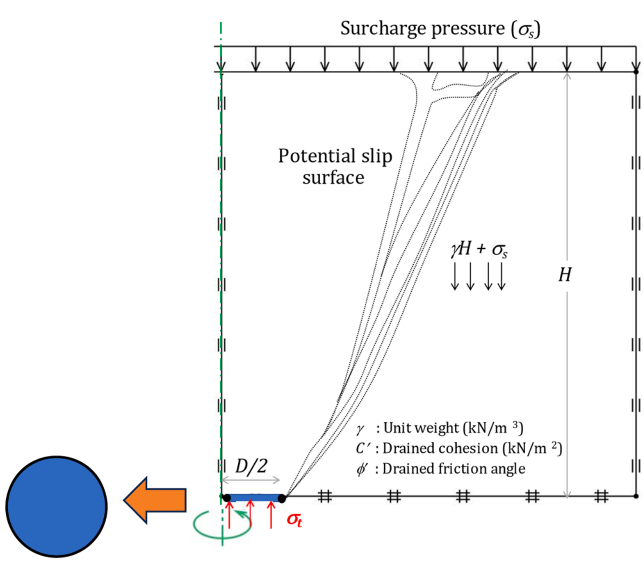

Fig. 1. A passive circular trapdoor in axisymmetry.

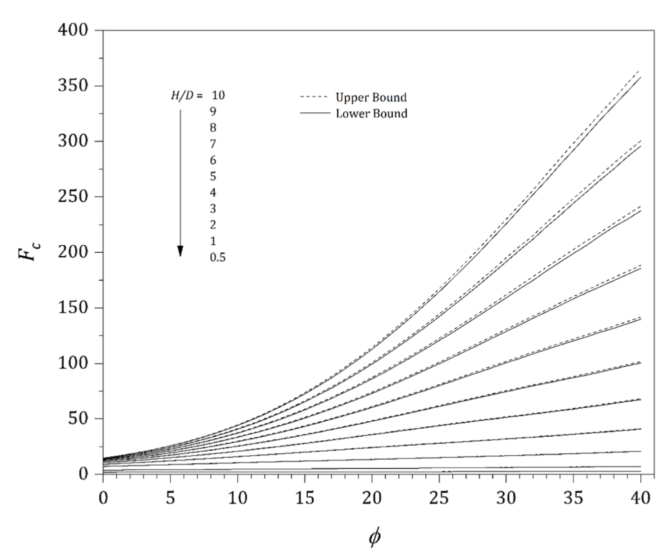

Fig. 3. F_c vs. ϕ (*LB* and *UB*) at various depth ratios (H/D = 0.5–10).

Table 1
F_c vs. ϕ (LB) at various depth ratios (H/D = 0.5–10).

ϕ	H/D (F_c, LB)										
	0.5	1	2	3	4	5	6	7	8	9	10
0	1.964	3.935	7.159	9.108	10.470	*11.521*	*12.362*	**13.074**	**13.685**	**14.218**	14.704
1	*1.980*	4.002	7.472	9.684	11.278	12.512	13.537	14.398	**15.156**	15.822	16.425
2	**1.997**	4.070	7.796	10.284	12.126	*13.591*	14.808	*15.858*	*16.790*	**17.615**	18.360
3	**2.014**	4.137	8.124	*10.912*	13.030	14.742	16.188	*17.471*	18.596	19.589	20.536
4	2.031	4.205	8.453	11.566	13.998	15.986	**17.700**	19.231	20.576	*21.834*	*22.973*
5	2.048	*4.273*	8.790	**12.239**	14.999	17.323	19.324	*21.146*	22.773	24.290	25.679
6	2.065	*4.340*	9.123	*12.935*	16.060	*18.737*	*21.117*	*23.236*	25.193	*26.989*	28.671
7	2.082	4.408	9.451	13.660	*17.200*	*20.258*	23.002	25.502	27.789	*29.986*	31.973
8	**2.099**	4.477	**9.787**	14.410	18.373	**21.853**	25.024	27.964	30.685	33.224	35.629
9	2.116	4.547	**10.120**	15.167	19.583	**23.553**	**27.209**	**30.612**	33.806	36.812	*39.676*
10	*2.113*	**4.616**	10.451	15.945	20.837	25.358	29.539	33.488	37.136	40.729	44.133
11	2.150	4.686	10.775	16.733	22.158	*27.242*	31.938	36.525	40.842	*44.912*	**48.923**
12	**2.166**	**4.756**	11.084	17.544	23.581	29.214	34.569	39.750	44.751	**49.502**	54.113
13	2.185	4.825	**11.402**	*18.360*	24.951	31.268	37.374	**43.255**	48.941	54.429	*59.850*
14	2.202	**4.896**	11.709	*19.191*	26.408	*33.400*	**40.173**	*46.870*	*53.395*	*59.707*	65.994
15	2.220	4.969	12.010	20.006	27.887	35.658	*43.274*	50.704	*58.115*	*65.368*	72.573
16	2.239	5.040	*12.297*	20.851	*29.434*	37.966	46.375	54.863	63.235	71.496	79.642
17	2.256	5.111	12.595	*21.677*	30.949	**40.366**	49.757	59.082	68.490	77.761	87.078
18	2.274	**5.185**	12.896	22.512	**32.568**	42.790	53.210	**63.601**	74.237	84.651	95.173
19	**2.293**	5.262	13.193	23.336	*34.143*	45.322	56.625	68.169	79.929	**91.739**	*103.756*
20	2.311	*5.337*	13.499	**24.151**	35.716	**47.879**	60.288	**73.028**	86.104	99.371	*112.719*
21	2.330	*5.414*	13.807	**24.947**	37.350	*50.490*	63.963	78.128	92.398	107.211	122.329
22	**2.348**	**5.490**	**14.113**	25.737	39.021	53.065	68.010	83.360	99.141	115.532	*132.283*
23	2.368	5.570	**14.432**	26.511	40.562	55.745	71.885	88.618	**106.047**	124.059	142.521
24	*2.387*	5.649	14.750	27.255	**42.229**	58.520	75.706	94.198	*113.143*	*132.912*	**153.504**
25	*2.407*	5.730	15.074	28.004	43.769	**61.183**	**79.925**	99.620	**120.537**	142.039	**164.454**
26	2.428	*5.811*	15.405	28.744	45.356	63.869	84.015	105.320	127.755	*151.694*	176.172
27	2.449	5.892	15.735	29.502	46.841	66.613	88.183	111.193	135.550	161.214	188.127
28	2.470	**5.977**	**16.071**	30.282	48.402	69.287	92.187	117.020	143.367	171.000	200.244
29	2.491	6.065	16.424	**31.059**	49.851	**71.885**	96.272	122.999	151.255	181.313	213.135
30	2.509	6.153	16.772	31.866	*51.366*	*74.453*	100.617	128.781	*159.101*	*191.585*	**225.787**
31	*2.534*	6.240	17.130	32.672	52.775	77.172	104.523	134.709	167.289	202.202	239.122
32	**2.557**	6.332	17.501	33.502	54.335	79.783	**108.640**	140.839	174.900	212.000	252.180
33	2.580	**6.428**	*17.872*	34.338	**55.807**	82.180	**112.598**	146.468	183.402	223.233	265.238
34	2.603	6.517	18.240	35.144	57.358	*84.670*	116.492	152.281	191.288	233.378	**279.121**
35	2.626	6.606	18.666	36.087	**58.910**	87.125	*120.372*	**158.201**	199.123	244.362	292.083
36	2.651	6.715	19.053	**37.010**	**60.559**	89.451	124.079	**163.774**	206.587	*254.672*	305.855
37	2.678	**6.822**	19.474	37.915	*62.070*	92.196	128.083	*169.262*	215.009	265.334	319.522
38	2.701	6.926	*19.875*	38.816	63.903	94.941	131.651	174.683	223.010	**275.104**	332.344
39	*2.731*	7.028	20.327	**39.768**	65.666	*97.678*	**135.691**	180.059	**229.777**	286.062	344.910
40	2.757	7.139	*20.784*	**40.823**	67.331	*100.431*	139.833	185.654	237.495	*295.811*	357.836

Table 2
F_c vs. ϕ (*UB*) at various depth ratios (H/D = 0.5–10).

ϕ	H/D (F_c, *UB*)										
	0.5	1	2	3	4	5	6	7	8	9	10
0	1.969	3.945	7.187	9.149	10.523	*11.578*	*12.416*	**13.109**	**13.722**	**14.251**	14.742
1	*1.985*	4.011	7.507	9.726	11.324	12.575	13.594	14.470	**15.205**	15.870	16.490
2	**2.002**	4.081	7.831	10.337	12.189	*13.664*	14.891	*15.948*	*16.875*	**17.658**	18.438
3	**2.019**	4.148	8.159	*10.970*	13.107	14.832	16.310	*17.575*	18.708	19.689	20.576
4	2.036	4.216	8.494	11.628	14.074	16.097	**17.839**	19.360	20.713	*21.936*	*23.089*
5	2.053	*4.283*	8.827	**12.310**	15.096	17.444	19.490	*21.308*	22.952	24.456	25.791
6	2.070	*4.353*	9.165	*13.013*	16.171	*18.894*	*21.256*	*23.430*	25.362	*27.226*	28.907
7	2.087	4.422	9.501	13.746	*17.313*	*20.421*	23.206	25.732	28.040	*30.218*	32.220
8	**2.104**	4.489	**9.840**	14.499	18.489	**22.054**	25.272	28.234	30.964	33.574	36.026
9	2.121	4.558	**10.169**	15.268	19.741	**23.779**	**27.476**	**30.926**	34.156	37.172	*40.088*
10	*2.138*	**4.629**	10.499	16.057	21.025	25.597	29.845	33.814	37.585	41.167	44.587
11	2.156	4.699	10.827	16.845	22.366	*27.505*	32.324	36.907	41.264	*45.432*	**49.462**
12	**2.173**	**4.768**	11.148	17.662	23.750	29.503	34.960	40.218	45.270	**50.108**	54.830
13	2.191	4.839	**11.459**	*18.495*	25.186	31.599	37.766	**43.731**	49.515	55.075	*60.626*
14	2.208	**4.910**	11.766	*19.316*	26.654	*33.784*	**40.685**	*47.452*	*54.059*	*60.479*	66.796
15	2.226	4.982	12.063	20.156	28.159	36.042	*43.783*	51.334	*58.874*	*66.292*	73.580
16	2.244	5.054	*12.357*	21.007	*29.693*	38.384	46.977	55.546	64.013	72.389	80.785
17	2.262	5.129	12.658	*21.836*	31.271	**40.794**	50.321	59.867	69.383	78.954	88.437
18	2.281	**5.202**	12.952	22.690	**32.865**	43.259	53.809	**64.434**	75.134	85.849	96.612
19	**2.299**	5.277	13.258	23.510	*34.472*	45.796	57.381	69.163	81.077	**93.128**	*105.301*
20	2.318	*5.352*	13.559	**24.320**	36.073	**48.377**	61.106	**74.019**	87.335	100.774	*114.473*
21	2.337	*5.429*	13.870	**25.126**	37.731	*51.044*	64.895	79.230	93.886	108.778	124.008
22	**2.356**	**5.508**	**14.178**	25.918	39.356	53.706	68.773	84.403	100.602	117.165	*134.183*
23	2.376	5.586	**14.500**	26.687	40.962	56.405	72.761	89.881	**107.664**	125.870	144.801
24	*2.396*	5.666	14.821	27.454	**42.584**	59.118	76.881	95.470	*114.845*	*134.956*	**155.711**
25	*2.416*	5.747	15.145	28.193	44.186	**61.858**	**80.943**	101.016	**122.308**	144.271	**167.210**
26	2.436	*5.829*	15.476	28.933	45.784	64.749	85.079	106.926	129.844	*154.003*	179.185
27	2.457	5.914	15.818	29.699	47.323	67.341	89.302	112.828	137.772	163.887	191.411
28	2.478	**5.999**	**16.162**	30.477	48.844	70.097	93.474	118.756	145.519	174.091	204.030
29	2.500	6.086	16.510	**31.264**	50.324	**72.781**	97.749	124.767	153.448	184.393	216.911
30	2.522	6.175	16.862	32.067	*51.851*	*75.486*	101.801	130.744	*161.907*	*195.291*	**229.957**
31	*2.544*	6.265	17.232	32.898	53.304	78.064	106.010	136.702	170.072	205.490	243.052
32	**2.567**	6.358	17.602	33.740	54.739	80.593	**110.140**	142.743	178.302	215.244	256.147
33	2.591	**6.452**	*17.979*	34.584	**56.306**	83.107	**114.070**	148.314	186.619	226.911	270.652
34	2.614	6.549	18.369	35.469	57.858	*85.630*	118.097	154.479	194.621	237.810	**284.499**
35	2.639	6.647	18.764	36.382	**59.472**	88.114	*122.002*	**160.324**	202.763	248.522	298.453
36	2.664	6.749	19.172	**37.323**	**61.102**	90.804	125.901	**165.892**	210.542	*259.126*	311.584
37	2.690	**6.853**	19.594	38.266	*62.806*	93.451	129.726	*171.763*	218.017	269.666	325.475
38	2.716	6.960	*20.130*	39.230	64.518	96.045	133.597	177.250	225.924	**280.215**	338.310
39	*2.734*	7.070	20.460	**40.187**	66.303	*98.804*	**137.599**	182.781	**233.903**	290.505	352.229
40	2.772	7.182	*20.911*	**41.215**	68.092	*101.658*	141.705	188.353	241.510	*300.483*	365.296

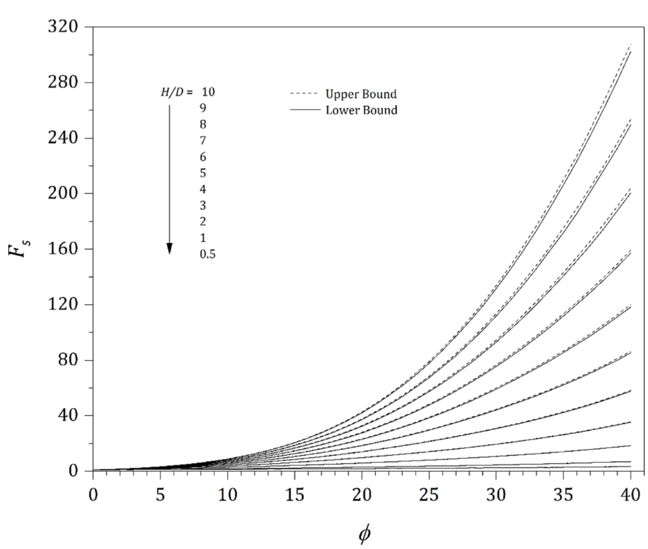

Fig. 4. F_s vs. ϕ (*LB* and *UB*) at various depth ratios (H/D = 0.5–10).

study aims to simulate an idealized blowout stage when a hole occurs in a pipe, causing hydraulic pressure to be exerted on the soil layer above. The hole was circular (Fig. 1), and the soil above it was cohesive-frictional. The hydraulic pressure was set as uniform. The results of this study can be used in practical engineering to evaluate the uplift pressure due to the scenario in which the pipeline burst-related ground stability is under blowout conditions.

To calculate the passive internal trapdoor pressure (σ_t) in cohesive-frictional soil under a blowout situation, Eq. (2) was employed. In this equation, the total compressive blowout pressure is equal to the cohesion, surcharge, and unit weight contributions. Noting similarity with the Terzaghi's bearing capacity approach, the respective factors for cohesion, surcharge, and unit weight are denoted as F_c, F_s, and F_γ. Unlike the Terzaghi's bearing capacity factors, these three factors are functions of both the soil friction angle and soil cover depth ratio (H/D). The variation in these two parameters results in various outcomes for the three stability factors, and this relationship can be expressed as shown in Eq. (3):

$$F_c, F_s, F_\gamma = f\left(\phi, \frac{H}{D}\right) \tag{3}$$

where F_c, denotes the drained cohesion factor; F_s, denotes the surcharge factor; F_γ, denotes the soil unit weight factor; H/D, is the soil cover-depth ratio; ϕ, is the soil internal friction angle.

FELA is a prominent technique used to solve a wide range of

Table 3
F_s vs. ϕ (LB) at various depth ratios (H/D = 0.5–10).

ϕ	H/D (F_S, LB)										
	0.5	1	2	3	4	5	6	7	8	9	10
0	1.002	1.004	1.007	1.009	1.010	*1.012*	*1.012*	**1.013**	**1.014**	**1.015**	1.016
1	*1.037*	1.074	1.138	1.179	1.208	1.231	1.250	1.266	**1.280**	1.292	1.303
2	**1.072**	1.146	1.280	1.369	1.436	*1.488*	1.532	*1.570*	*1.603*	**1.633**	1.660
3	**1.108**	1.221	1.434	*1.583*	1.696	1.788	1.865	*1.933*	1.994	2.047	2.097
4	1.144	1.298	1.599	1.820	1.992	2.134	**2.257**	2.364	2.459	*2.549*	*2.630*
5	1.181	*1.378*	1.777	**2.083**	2.328	2.532	2.713	*2.871*	3.016	3.148	3.267
6	1.219	*1.461*	1.968	*2.373*	2.706	*2.988*	*3.240*	*3.466*	3.627	*3.863*	4.044
7	1.258	1.546	2.171	2.692	*3.128*	*3.505*	3.849	4.157	4.440	*4.712*	4.960
8	**1.297**	1.634	**2.386**	3.040	3.597	**4.095**	4.541	4.957	5.347	5.707	6.046
9	1.337	1.725	**2.610**	3.416	4.123	**4.755**	**5.339**	**5.879**	6.389	6.870	*7.326*
10	*1.378*	**1.818**	2.852	3.828	4.698	5.494	6.241	6.928	7.588	8.225	8.819
11	1.420	1.915	3.103	4.270	5.337	*6.318*	7.251	8.134	8.971	*9.769*	**10.563**
12	**1.463**	**2.016**	3.368	4.744	6.030	7.240	8.395	9.488	10.553	**11.571**	12.567
13	1.507	2.119	**3.643**	*5.258*	6.796	8.254	9.667	**11.025**	12.341	13.630	*14.860*
14	1.550	**2.226**	3.931	*5.805*	7.611	*9.367*	**11.065**	*12.736*	*14.359*	*15.945*	17.515
15	1.597	2.336	4.230	6.387	8.506	10.595	*12.643*	14.658	*16.647*	*18.580*	20.521
16	1.644	2.450	*4.538*	6.998	*9.479*	11.932	14.337	16.777	19.203	21.549	23.886
17	1.692	2.569	4.862	*7.650*	10.518	**13.374**	16.253	19.113	21.963	24.872	27.725
18	1.741	**2.690**	5.202	8.337	**11.610**	14.995	18.307	**21.729**	25.144	28.584	32.031
19	**1.792**	2.817	5.557	9.053	*12.782*	16.638	20.582	24.583	28.648	**32.663**	*36.818*
20	1.844	*2.948*	5.925	**9.811**	14.039	**18.464**	23.000	**27.651**	32.426	37.235	*42.129*
21	1.897	*3.084*	6.313	**10.601**	15.395	*20.432*	25.630	31.076	36.566	42.271	48.002
22	**1.951**	**3.224**	**6.716**	11.424	16.802	22.498	28.494	34.733	41.173	47.725	*54.484*
23	2.007	3.369	**7.139**	12.275	18.280	24.727	31.576	38.744	**46.119**	53.737	61.615
24	*2.066*	3.519	7.582	13.163	**19.799**	27.100	34.839	42.990	*51.509*	*60.388*	**69.183**
25	*2.125*	3.676	8.044	14.091	21.458	**29.595**	**38.376**	47.591	**57.345**	67.340	**77.791**
26	2.187	*3.840*	8.527	15.049	23.166	32.243	42.007	52.541	63.473	*75.169*	87.094
27	2.250	4.008	9.036	16.063	24.914	34.998	46.025	57.755	70.272	83.233	97.133
28	2.315	**4.185**	**9.565**	17.118	26.781	37.922	50.077	63.253	77.268	92.291	107.803
29	2.382	4.368	10.116	**18.252**	28.708	**40.970**	54.522	69.240	85.057	101.712	119.100
30	2.453	4.558	10.704	19.423	*30.720*	*44.091*	59.142	75.445	*92.983*	*111.844*	**131.644**
31	*2.525*	4.757	11.315	20.671	32.766	47.458	64.005	82.075	101.648	122.645	144.660
32	**2.600**	4.965	11.957	21.972	34.961	50.838	**69.018**	88.919	110.614	133.999	158.739
33	2.677	**5.180**	*12.631*	23.348	**37.265**	54.449	**74.227**	96.227	120.153	146.095	173.555
34	2.758	5.406	13.332	24.769	39.728	*58.211*	79.620	103.779	130.418	159.104	**189.677**
35	2.841	5.640	14.082	26.268	**42.334**	62.108	*85.504*	**111.816**	140.696	171.902	206.236
36	2.928	5.886	14.852	**27.877**	**44.977**	66.260	91.441	**120.241**	151.658	*185.727*	223.410
37	3.020	**6.148**	15.691	29.615	*47.934*	70.593	97.426	*128.785*	162.781	201.272	241.787
38	3.115	6.418	*16.565*	31.408	50.969	75.255	104.169	137.728	174.701	**216.861**	261.168
39	*3.240*	6.699	17.473	**33.321**	54.212	*79.873*	**111.121**	147.108	**187.488**	232.440	281.027
40	3.317	7.003	*18.454*	**35.319**	57.598	*85.280*	118.265	157.128	200.385	*249.389*	302.188

Table 4
F_s vs. ϕ (*UB*) at various depth ratios ($H/D = 0.5$–10).

ϕ	*H/D* (F_S, *UB*)										
	0.5	1	2	3	4	5	6	7	8	9	10
0	1.002	1.004	1.007	1.009	1.010	*1.012*	*1.012*	**1.013**	**1.014**	**1.015**	1.016
1	*1.037*	1.074	1.139	1.180	1.209	1.232	1.251	1.267	**1.280**	1.293	1.304
2	**1.072**	1.147	1.281	1.371	1.438	*1.491*	1.535	*1.573*	*1.606*	**1.636**	1.663
3	**1.108**	1.222	1.436	*1.586*	1.700	1.793	1.871	*1.939*	2.000	2.054	2.103
4	1.144	1.299	1.602	1.825	1.998	2.142	**2.265**	2.374	2.470	*2.558*	*2.641*
5	1.182	*1.379*	1.781	**2.089**	2.336	2.544	2.726	*2.887*	3.032	3.165	3.289
6	1.220	*1.462*	1.973	*2.381*	2.716	*3.004*	*3.259*	*3.487*	3.695	*3.890*	4.068
7	1.258	1.547	2.177	2.702	*3.143*	*3.527*	3.874	4.187	4.473	*4.745*	4.990
8	**1.298**	1.635	**2.393**	3.052	3.619	**4.120**	4.577	4.996	5.387	5.754	6.095
9	1.338	1.727	**2.622**	3.433	4.147	**4.790**	**5.380**	**5.925**	6.440	6.928	*7.393*
10	*1.379*	**1.821**	2.863	3.847	4.729	5.535	6.291	6.997	7.660	8.295	8.911
11	1.421	1.918	3.116	4.294	5.372	*6.375*	7.318	8.212	9.058	*9.878*	**10.666**
12	**1.464**	**2.019**	3.381	4.774	6.075	7.302	8.470	9.583	10.663	**11.691**	12.689
13	1.508	2.122	**3.658**	*5.288*	6.841	8.327	9.758	**11.136**	12.472	13.771	*15.055*
14	1.553	**2.229**	3.947	*5.838*	7.675	*9.457*	**11.186**	*12.875*	*14.532*	*16.142*	17.698
15	1.599	2.340	4.245	6.426	8.576	10.686	*12.769*	14.814	*16.831*	*18.814*	20.766
16	1.646	2.455	*4.558*	7.044	*9.547*	12.046	14.520	16.977	19.410	21.791	24.212
17	1.694	2.573	4.881	*7.702*	10.592	**13.505**	16.438	19.363	22.271	25.187	28.067
18	1.743	**2.696**	5.223	8.393	**11.709**	15.105	18.536	**21.976**	25.448	28.928	32.426
19	**1.794**	2.823	5.577	9.119	*12.908*	16.814	20.813	24.878	28.944	**33.091**	*37.307*
20	1.846	*2.954*	5.951	**9.879**	14.173	**18.672**	23.308	**28.029**	32.849	37.740	*42.657*
21	1.900	*3.090*	6.337	**10.673**	15.520	*20.655*	25.987	31.478	37.104	42.787	48.701
22	**1.954**	**3.231**	**6.744**	11.504	16.950	22.767	28.871	35.200	41.707	48.382	*55.155*
23	2.011	3.377	**7.168**	12.359	18.447	25.023	31.973	39.217	**46.766**	54.495	62.523
24	*2.069*	3.529	7.613	13.252	**20.014**	27.418	35.298	43.560	*52.193*	*61.160*	**70.430**
25	*2.129*	3.686	8.079	14.179	21.663	**29.925**	**38.831**	48.231	**58.082**	68.370	**79.059**
26	2.191	*3.850*	8.566	15.143	23.381	32.634	42.616	53.246	64.417	*76.176*	88.511
27	2.255	4.019	9.075	16.169	25.168	35.422	46.591	58.566	71.353	84.586	98.542
28	2.320	**4.196**	**9.610**	17.237	27.032	38.373	50.833	64.221	78.596	93.655	109.661
29	2.388	4.380	10.170	**18.364**	28.956	**41.443**	55.296	70.295	86.234	103.400	121.162
30	2.458	4.572	10.756	19.557	*30.993*	*44.671*	59.936	76.542	*94.479*	*113.669*	**133.797**
31	*2.531*	4.772	11.370	20.880	33.094	48.008	64.868	83.255	103.365	124.601	147.222
32	**2.607**	4.980	12.015	22.118	35.299	51.485	**69.972**	90.361	112.637	136.487	161.925
33	2.685	**5.196**	*12.695*	23.501	**37.630**	55.099	**75.287**	97.690	122.288	148.501	176.997
34	2.766	5.423	13.407	24.981	40.164	*58.836*	80.853	105.382	132.395	161.527	**193.068**
35	2.850	5.661	14.159	26.511	**42.737**	62.894	*86.603*	**113.438**	143.136	175.324	210.009
36	2.938	5.981	14.950	**28.141**	**45.470**	66.994	92.612	**121.832**	154.196	*189.434*	227.185
37	3.030	**6.171**	15.786	29.848	*48.378*	71.524	98.871	*130.545*	165.856	204.478	246.235
38	3.125	6.444	*16.663*	31.662	51.472	76.111	105.564	139.759	177.939	**220.063**	266.187
39	*3.224*	6.732	17.592	**33.609**	54.764	*81.110*	**112.609**	149.176	**190.694**	236.396	286.687
40	3.328	7.034	*18.564*	**35.635**	58.220	*86.403*	120.111	159.229	203.856	*253.377*	307.655

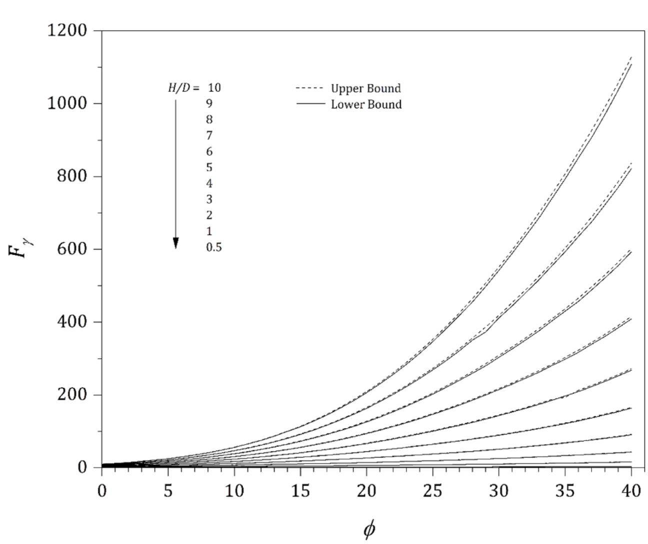

Fig. 5. F_γ vs. ϕ (*LB* and *UB*) at various depth ratios ($H/D = 0.5$–10).

geotechnical stability problems. This is an effective approach for computing the limit load with a precise upper–lower bound solution. Sloan [16] discussed the historical development of FELA for assessing soil stability, starting from the earliest FELA initiatives that employed linear programming [17,18] up to the most recent important advancements that used non-linear programming [19–21]. OptumG2 is the most recently developed FELA program. This software has been used effectively to solve several stability problems in geotechnical engineering [22–24]. It was used to perform a parametric analysis in this study to establish UB and LB solutions for the drained passive circular trapdoor. Within OptumG2, the UB elements have three nodes that provide an unidentified velocity linear approximation, whereas the LB elements have three nodes that provide an unidentified stress linear approximation with stress discontinuity possibilities at the overlaying triangular edges. A perfectly plastic Mohr–Coulomb material was utilized in combination with a flow rule to replicate the solid components that constitute the drained soil. Further details on the FELA formulation can be found in Shiau and Al-Asadi [13].

Fig. 2 shows a typical numerical model, boundary condition, and adaptive mesh for F_γ analysis ($H/D = 3$). The drained passive circular trapdoor was placed under axisymmetric conditions, where the axial symmetry line was set on the left soil domain border. The model required only half of the circular trapdoor, owing to the axisymmetric assumption. The boundary conditions for the FELA analysis were set as follows: the two vertical borders were set as roller supports with no vertical motion restriction; the horizontal border (model base) was set as

Table 5
F_γ vs. ϕ (LB) at various depth ratios (H/D = 0.5–10).

ϕ	H/D (F_γ, LB)										
	0.5	1	2	3	4	5	6	7	8	9	10
0	0.501	1.004	2.014	3.026	4.040	*5.055*	*6.074*	**7.094**	**8.112**	**9.128**	10.160
1	*0.510*	1.090	2.158	3.335	4.552	5.790	7.059	8.340	**9.632**	10.935	12.260
2	**0.519**	1.076	2.308	3.668	5.112	*6.615*	8.169	*9.769*	*11.392*	**13.022**	14.730
3	**0.528**	1.113	2.466	*4.025*	5.728	7.530	9.436	*11.408*	13.408	15.522	17.690
4	0.537	1.150	2.628	4.412	6.400	8.555	**10.852**	13.277	15.792	*18.399*	*21.130*
5	0.546	*1.189*	2.800	**4.823**	7.140	9.690	12.461	*15.399*	18.488	21.727	25.140
6	0.556	*1.229*	2.976	*5.261*	7.944	*10.950*	*14.250*	*17.801*	21.568	*25.549*	29.770
7	0.565	1.270	3.162	5.726	*8.812*	*12.335*	16.242	20.497	25.056	*29.919*	35.100
8	**0.575**	1.311	**3.354**	6.218	9.752	**13.845**	18.451	23.536	29.008	34.901	41.210
9	0.584	1.354	**3.554**	6.743	10.764	**15.505**	**20.888**	**26.905**	33.488	40.567	*48.140*
10	*0.594*	**1.398**	3.760	7.292	11.860	17.310	23.601	30.679	38.424	46.942	56.120
11	0.604	1.443	3.976	7.867	13.008	*19.260*	26.561	34.811	43.968	*54.056*	**65.110**
12	**0.615**	**1.489**	4.202	8.473	14.256	21.390	29.760	39.426	50.136	**61.951**	75.150
13	0.625	1.537	**4.434**	*9.106*	15.580	23.605	33.295	**44.419**	56.952	70.881	*86.480*
14	0.636	**1.585**	4.674	*9.757*	16.964	*26.085*	**37.119**	*49.888*	*64.552*	*80.782*	99.840
15	0.647	1.635	4.926	10.444	18.432	28.705	*41.255*	55.966	*72.640*	*91.691*	112.690
16	0.658	1.687	*5.188*	11.155	*19.984*	31.470	45.702	62.437	81.664	103.633	128.230
17	0.669	1.739	5.462	*11.905*	21.616	**34.445**	50.408	69.447	91.528	117.005	144.950
18	0.680	**1.794**	5.740	12.678	**23.312**	37.575	55.486	**77.080**	102.208	131.259	164.110
19	**0.692**	1.850	6.038	13.509	*25.088*	40.875	60.846	85.147	113.520	**146.664**	*184.030*
20	0.704	*1.907*	6.340	**14.352**	26.944	**44.365**	66.693	**94.034**	125.960	163.426	*206.440*
21	0.716	*1.967*	6.660	**15.237**	28.912	*48.080*	72.725	103.214	139.080	181.942	230.560
22	**0.729**	**2.028**	**6.988**	16.179	30.884	51.885	79.280	113.347	153.664	201.439	*256.310*
23	0.741	2.091	**7.328**	17.163	33.008	55.925	85.930	123.655	**169.032**	222.716	283.930
24	*0.755*	2.156	7.694	18.176	**35.204**	60.130	93.175	134.818	*185.416*	*245.207*	**314.250**
25	*0.768*	2.223	8.058	19.226	37.548	**64.520**	**100.444**	146.541	**202.488**	269.056	**346.720**
26	0.782	*2.295*	8.450	20.360	39.912	69.040	108.649	159.223	220.576	*294.155*	381.760
27	0.796	2.366	8.858	21.533	42.500	73.775	116.609	171.863	240.112	321.124	418.490
28	0.811	**2.440**	**9.270**	22.753	45.168	78.635	124.676	185.658	259.648	350.764	455.790
29	0.826	2.520	9.712	**24.022**	47.960	**83.840**	133.667	199.951	280.080	373.022	498.290
30	0.841	2.597	10.172	25.390	*50.892*	*89.365*	143.157	214.839	*303.440*	*411.879*	**542.580**
31	*0.858*	2.681	10.658	26.791	53.968	95.145	153.139	229.867	326.672	444.874	589.000
32	**0.874**	2.768	11.160	28.275	57.520	101.200	**163.187**	245.707	350.848	480.036	636.610
33	0.891	**2.861**	*11.678*	29.823	**60.620**	107.570	**173.697**	262.101	375.472	515.791	685.270
34	0.909	2.954	12.212	31.443	64.260	*114.400*	185.312	280.700	403.312	554.685	**739.550**
35	0.927	3.048	12.808	33.173	**68.148**	121.115	*197.419*	**298.193**	430.140	593.498	793.520
36	0.946	3.152	13.404	**35.012**	**72.104**	128.830	209.178	**317.276**	456.968	*635.414*	851.110
37	0.967	**3.258**	14.034	36.899	*76.256*	136.805	223.061	*339.713*	488.632	675.405	907.160
38	0.988	3.367	*14.710*	38.869	80.928	145.410	237.155	360.462	521.176	**722.248**	969.910
39	*1.009*	3.485	15.436	**41.050**	85.244	*153.955*	**252.281**	384.433	**555.240**	769.847	1036.530
40	1.031	3.609	*16.170*	**43.224**	90.572	*163.845*	268.055	408.810	592.816	*821.493*	1107.800

Table 6
F_γ vs. ϕ (*UB*) at various depth ratios (H/D = 0.5–10).

ϕ	H/D (F_γ, *UB*)										
	0.5	1	2	3	4	5	6	7	8	9	10
0	0.501	1.004	2.014	3.026	4.040	*5.055*	*6.074*	**7.094**	**8.112**	**9.128**	10.160
1	*0.510*	1.039	2.158	3.335	4.552	5.790	7.059	8.340	**9.632**	10.935	12.260
2	**0.519**	1.076	2.310	3.671	5.116	*6.620*	8.175	*9.776*	*11.408*	**13.049**	14.760
3	**0.528**	1.113	2.468	*4.031*	5.732	7.545	9.442	*11.415*	13.440	15.549	17.990
4	0.537	1.151	2.632	4.415	6.412	8.575	**10.870**	13.298	15.816	*18.435*	*21.150*
5	0.546	*1.190*	2.802	**4.829**	7.156	9.715	12.497	*15.448*	18.536	21.790	25.190
6	0.556	*1.230*	2.980	*5.270*	7.968	*10.990*	*14.304*	*17.864*	21.616	*25.656*	29.880
7	0.565	1.271	3.166	5.741	*8.488*	*12.385*	16.333	20.609	25.184	*30.054*	35.250
8	**0.575**	1.312	**3.358**	6.239	9.792	**13.920**	18.571	23.662	29.208	35.117	41.480
9	0.585	1.355	**3.560**	6.764	10.812	**15.595**	**21.044**	**27.087**	33.664	40.809	*48.550*
10	*0.595*	**1.399**	3.768	7.316	11.912	17.420	23.752	30.903	38.736	47.284	56.510
11	0.605	1.444	3.984	7.900	13.088	*19.390*	26.771	35.084	44.376	*54.550*	**65.580**
12	**0.615**	**1.491**	4.210	8.506	14.336	21.535	30.024	39.769	50.640	**62.644**	75.780
13	0.626	1.538	**4.444**	*9.145*	15.668	23.835	33.601	**44.846**	57.592	71.673	*87.240*
14	0.636	**1.587**	4.688	*9.808*	17.076	*26.305*	**37.419**	*50.448*	*65.184*	*81.736*	100.040
15	0.647	1.637	4.940	10.492	18.572	28.955	*41.603*	56.499	*73.528*	*92.725*	113.910
16	0.658	1.689	*5.204*	11.209	*20.124*	31.775	46.092	63.130	82.768	104.982	129.920
17	0.669	1.742	5.476	*11.953*	21.776	**34.770**	50.936	70.266	92.768	118.103	147.180
18	0.681	**1.797**	5.758	12.753	**23.508**	37.935	56.086	**77.983**	103.576	132.887	166.080
19	**0.693**	1.853	6.054	13.572	*25.292*	41.280	61.615	86.176	115.320	**148.741**	*186.940*
20	0.705	*1.911*	6.360	**14.433**	27.172	**44.815**	67.455	**95.161**	127.936	165.926	*209.500*
21	0.717	*1.970*	6.680	**15.333**	29.120	*48.540*	73.649	104.629	141.448	184.406	233.930
22	**0.730**	**2.032**	**7.010**	16.269	31.144	52.400	80.168	114.643	156.032	204.406	*260.500*
23	0.743	2.095	**7.358**	17.256	33.268	56.505	87.101	125.385	**171.560**	225.791	289.050
24	*0.756*	2.161	7.718	18.284	**35.472**	60.725	94.346	136.856	*187.944*	*248.849*	**319.780**
25	*0.769*	2.229	8.092	19.358	37.796	**65.160**	**101.921**	148.606	**205.568**	273.174	**352.680**
26	0.783	*2.299*	8.482	20.492	40.276	69.700	109.850	161.176	224.400	*299.164*	387.630
27	0.797	2.372	8.890	21.662	42.812	74.455	118.247	174.307	243.672	326.978	425.050
28	0.812	**2.447**	**9.316**	22.906	45.524	79.490	126.675	188.179	264.240	356.520	464.880
29	0.828	2.525	9.760	**24.193**	48.360	**84.765**	135.678	202.535	286.056	386.808	507.320
30	0.843	2.606	10.222	25.555	*51.376*	*90.280*	145.144	217.612	*308.880*	*418.597*	**551.870**
31	*0.859*	2.690	10.708	26.986	54.496	96.140	154.916	233.074	331.936	453.966	598.410
32	**0.876**	2.777	11.214	28.482	57.760	102.280	**165.192**	249.622	356.280	488.237	647.140
33	0.893	**2.868**	*11.744*	30.054	**61.252**	108.765	**176.224**	266.513	381.928	525.063	699.320
34	0.911	2.963	12.302	31.710	64.856	*115.680*	187.659	284.300	409.032	563.121	**752.620**
35	0.930	3.061	12.888	33.452	**68.788**	122.880	*193.619*	**303.088**	436.784	604.191	807.420
36	0.949	3.164	13.496	**35.282**	**72.856**	130.525	212.551	**323.081**	466.080	*645.207*	866.560
37	0.969	**3.272**	14.144	37.217	*77.140*	138.605	226.044	*344.433*	497.248	688.957	926.520
38	0.990	3.384	*14.820*	39.256	81.672	147.110	240.516	366.513	529.728	**735.845**	989.990
39	*1.011*	3.501	15.536	**41.416**	86.508	*156.175*	**255.732**	390.399	**564.840**	785.000	1056.190
40	1.034	3.625	*16.284*	**43.680**	91.572	*165.775*	271.957	415.511	601.976	*836.745*	1127.550

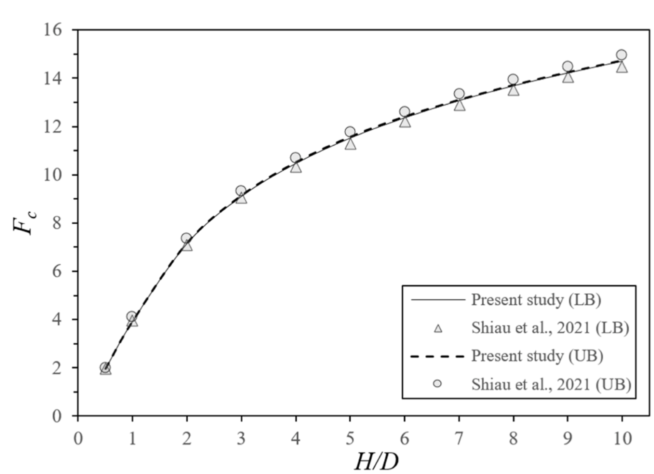

Fig. 6. Current study comparison with that of Shiau et al. [26] (LB and UB) at various depth ratios (H/D = 0.5–10) with $\phi = 0°$.

a fixed support where both vertical and horizontal motion were restricted; lastly, the top ground surface was set as a free surface without restriction. Note that regarding the roller support stress boundary conditions, shear stresses are constrained to zero, whereas normal stresses are unconstrained. For a fixed support at the bottom boundary, both shear and normal stresses were constrained to zero. Model domain dimensions were determined to be sufficiently large to guarantee that the soil motions were accurately localized within the specified domain.

Moreover, the FELA program incorporates an adaptive mesh refinement feature, which was created by Ciria et al. [25], to mitigate errors and enhance finding accuracy. Adaptive meshing technique application, in which the number of elements is automatically increased in zones with large plastic shear strains, considerably improves simulation computational performance. To minimize the confining discrepancies between the UB and LB solutions, a load multiplier technique and adaptive mesh refinement were implemented [16].

As shown in Fig. 2, automated mesh adaptivity was conducted to compute the circular trapdoor drained passive stability UB and LB solutions. The sensitivity zone gradient allows for direct intense plastic shearing strain regional observation. Three adaptive iteration stages were used in all the studies as suggested in the software, ensuring that this value was adequate to generate a reliable outcome. The initial 3000-component mesh was gradually increased to a final 5000-component

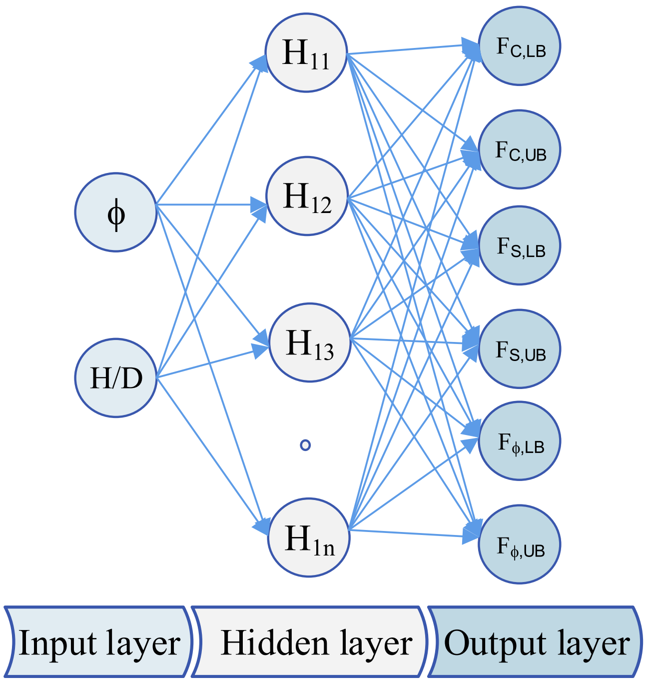

Fig. 7. ANN model structure.

mesh over three iteration rounds.

3. Results and discussion

A series of parametric studies regarding the LB and UB analysis three stability factors F_c, F_s, and F_γ were conducted using two dimensionless parameters, namely the cover-depth ratio (H/D) and drained frictional angle (ϕ). The selected parameters covered the $H/D = 0.5$–10 and $\phi =$ 0–40 ranges, respectively.

Cohesion factor F_c, results for the H/D and ϕ value ranges are shown in Fig. 3. Both UB and LB results are shown in the Figure. The confidence level with the produced results has been substantially increased by the fact that UB and LB results can bracket the ``true'' solutions within 1 %. It is recommended that future solutions using various techniques be compared with the results obtained in this study. In general, a non-linear relationship between F_c and ϕ was observed, where the greater the ϕ, the larger is the F_c. A larger gradient showing a strong rate of increase was also observed in the $\phi = 30$–40 range. In addition, regarding the shallow trapdoor, the variation in ϕ had little effect on F_c values. This can be explained by understanding material arching, particularly in deep trapdoors. There is insufficient length in shallow trapdoors for material arching to develop. The complete F_c result list is provided in Tables 1 and 2.

Regarding the surcharge factor F_s, numerical results on the drained frictional angle ϕ effects in the $H/D = 0.5$–10 range are shown in Fig. 4. Similar to F_c (Fig. 3), a non-linear relationship between F_s and ϕ was observed. For frictionless soils ($\phi = 0$) under undrained conditions, F_s was exactly 1 for all H/D values. As H/D increased (trapdoor depth increased), the soil arching phenomenon began to increase, especially when ϕ increased from 10 to 40. However, negligible effects were reported at shallow depths such as $H/D = 0.5$, and 1, as shown in the Figure. The complete F_s result list is provided in Tables 3 and 4.

Finally, Fig. 5 shows the drained frictional angle ϕ effects on F_γ at the various depth ratios ($H/D = 0.5$–10). Similar trends with F_c and F_s (see Figs. 3 and 4) were observed in this "passive" study. The deeper the trapdoor, the greater are the F_γ values. Moreover, the non-linear increasing F_γ values were most pronounced at greater depth ratios (H/D). The minimum 0.5 F_γ value was obtained at $\phi = 0$ and $H/D = 0.5$. The complete F_γ result list is provided in Tables 5 and 6.

However, to confirm the FELA results obtained in this study, a comparison was made with those of Shiau et al. [26]. In their study, a passive trapdoor three-dimensional stability factor was provided. The cohesion factor (F_c) results were compared with those of the selected $\phi = 0$ and $H/D = 0.5$–10 cases in the current study. Specifically, the two investigations exhibited excellent agreement for both the UB and LB solutions, as illustrated in Fig. 6, demonstrating that the proposed stability solutions are accurate and reliable.

A simple example

An underground circular cavity in an urban area with a 100 kPa surcharge loading ($\sigma_s = 100$ kPa) had a 2 m width B (or diameter D) and a 16 m cover depth (H). The soil was found to have a ($c = 17$ kPa) cohesion with a 16 kN/m^3 unit weight. The internal friction angle was set at 30°. The critical inner blowout pressure was determined using three stability factors.

Solution: For $H/B = 8$ and $\phi = 30^\circ$, Tables 1, 3, and 5 provide the LB values; $F_c = 159.101$, $F_s = 92.983$, and $F_\gamma = 303.440$. Substituting all the parameters into Eq. (2), σ_t was calculated as 21,713.09 kPa. The actual computer analysis using these parameters gives a 21,944.08 kPa value, which is extremely close to that of the tabular solution. Thus, the tabular approach is both reliable and convenient, with differences within 1 %, suggesting that practical engineers can use it with confidence.

4. ANN predictive model

Over previous years, several machine learning approaches have been developed and can be classified into four groups: neuron-based (ANN, ANFIS(adaptive-network-based fuzzy inference systems)), kernel-based (SVM (support vector machine), KNEA (kernel-based non-linear extension of Arps decline)), tree-based (M5Tree, XGBoost), and curve-based (MARS(multivariate adaptive regression splines)) models. Although the XGBoost or MARS models are considered better machine learning approaches [27–29], ANN is generally recognized as a productive statistical learning method for addressing regression and classification problems and providing explicit predictive equations. For instance, it has been extensively utilized in various fields of study, from construction management to structural analysis [30,31]. Geotechnology has played a vital role in predicting soil and structural comportment, such as slope stability [32], ring foundation uplift resistance [33], and pipeline pull-out capacity [34]. Thus, the ANN model was adopted in this study.

A typical ANN framework in which numerous layered nodes are simultaneously manipulated is shown in Fig. 7. The input layer is for the

Table 7
Input parameter statistical properties for set training, testing, and validation.

Variable	Training set				Testing set				Validation set			
	Min	Max	Mean	SD	Min	Max	Mean	SD	Min	Max	Mean	SD
ϕ	0.0	40	20.39	11.72	0.0	40	20.43	11.70	0.0	40	17.78	12.21
H/D	0.5	10	5.03	3.09	0.5	10	4.71	3.06	0.5	10	5.46	3.09

*Note: SD, standard deviation.

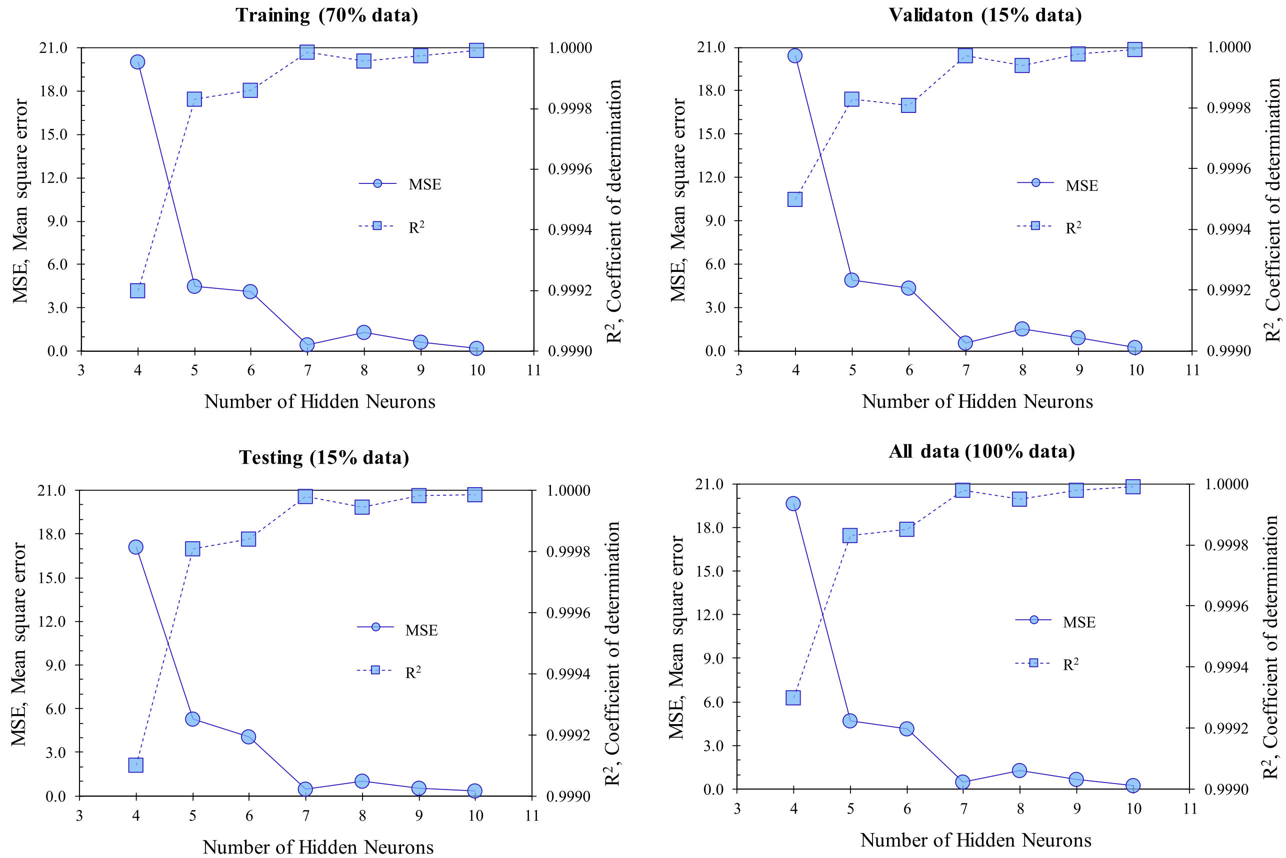

Fig. 8. Convergency study – MSE and R^2 versus the number of hidden neurons.

unprocessed dataset, whereas the hidden layers obtain all computations that need to be performed. Finally, the output layer generates the model predictions [35].

As the process began, a coincidental value was assigned to individual neuron weights and biases. These values were then modified after each iteration to improve model performance. In addition, the procedure included a comparison between the desired objective and the actual result as well as the loss value calculation. At each hidden node, the activation functions translated the weighted inputs and biases into values to be used in the following layer. Owing to its robust capacity to accelerate the training process, the hyperbolic tangent transfer function shown in Eq. (4) was chosen to calculate the hidden layer output. In addition, a wide variety of techniques, such as Levenberg–Marquardt (LM), stochastic gradient descent, and Bayesian regularization, were introduced for ANN optimization. As recommended in [36,37], the LM algorithm was employed to adjust the weight and bias numbers.

$$\mathrm{tansig}(x) = \tanh(x) = \frac{2}{1+\mathrm{e}^{-2x}} - 1 \tag{4}$$

$$\mathrm{Prediction} = \sum_{i=1}^{N_h} W^{2,i}\mathrm{tansig}\left(\sum_{j=1}^{J} W^{1,i}x^j + b^{1,i}\right) + b^{2,i} \tag{5}$$

All the results from the FELA method were used to construct the ANN models. The input parameters comprise the drained friction angle ϕ and soil cover depth ratio H/D, whereas the output features comprise the LB and UB solution three stability factors F_c, F_s, and F_γ. The ANN model analysis encompassed 451 design cases that corresponded to H/D depth ratios at (0.5, 1.0, 2.0, 3.0, 4.0, 6.0, 7.0, 8.0, 9.0, and 10.0) and ϕ ranging from 0 to 40 (totaling 41 cases). Notably, 70 % of the data are used for the training set, 15 % for the validation set, and 15 % for the test set. Specifically, all data for training ANN are listed in Tables 1–6, in which the bold numbers represent the test set, and the italicized numbers are used for validation. The four statistical data properties in each set, comprising boundaries, mean, and standard deviation, are listed in Table 7, revealing the two input parameter approximate values in the three groups.

The number of nodes effect in a model hidden layer is an important consideration when selecting an optimal ANN model. The mean squared error (MSE) and coefficient of determination (R^2) were used to assess optimal ANN model effectiveness [38]. The relationships between the number of hidden neurons, R^2, and MSE for training (70 % of the data), validation (15 % of the data), testing (15 % of the data), and all (100 % of the data) are illustrated in Fig. 8. The numerical results showed a noticeable increase in R^2 and a dramatic decrease in MSE when the number of hidden nodes was increased to seven. Thereafter, they remained approximately constant, despite slight fluctuations. Therefore, seven neurons were used in all analyses. The corresponding values for the seven neurons are $R^2 = 0.99998$ and MSE = 0.47030.

The optimal model weight and bias values, as listed in Table 8, were used to develop accurate equations to estimate the three stability factors (UB and LB). The hyperbolic tangent function Eqs. (4) and (5) was applied to construct the forecasting function that considers the ϕ and H/D input parameters. The formulae for calculating F_c, F_s, and F_γ (LB and UB) are shown in Eqs. (6)–(11).

$$F_{c,LB} = 1.1767N_1 + 2.7713N_2 + 12.9184N_3 + 10.0937N_4 - 5.0884N_5 - 1.6165N_6 + 2.9652N_7 + 0.6282 \tag{6}$$

Table 8
Optimal ANN model weight and bias values (seven neurons).

Neuron	Input variables			Output											
	W^1		b^1	W^2						b^2					
	ϕ	H/D		F											
1	1.1786	0.9919	−2.8154	1.1767	1.1934	2.1949	2.2006	2.8602	2.8631	0.6282	0.6403	1.7572	1.7615	2.1109	2.1130
2	0.3020	0.8066	−0.7231	2.7714	2.7494	3.4828	3.4682	1.4415	1.4243						
3	−0.7221	0.2695	0.8450	12.9185	12.9753	1.7379	1.8026	10.6803	10.7605						
4	0.6964	−0.0273	−0.6421	10.0937	10.1077	4.4450	4.4866	7.9057	7.9666						
5	−0.7325	0.4543	1.0060	−5.0885	−5.1286	0.6800	0.6495	−4.5930	−4.6255						
6	0.1593	0.9393	−0.8591	−1.6165	−1.6025	−2.0105	−1.9972	−0.6669	−0.6506						
7	−0.5917	−0.3726	0.3939	2.9653	2.9590	2.9360	2.9439	2.3473	2.3605						

$$F_{c,UB} = 1.1934N_1 + 2.7494N_2 + 12.9753N_3 + 10.1077N_4 - 5.1286N_5 - 1.6025N_6 + 2.9590N_7 + 0.6403 \tag{7}$$

$$F_{s,LB} = 2.1949N_1 + 3.4828N_2 + 1.7379N_3 + 4.4450N_4 + 0.6800N_5 - 2.0105N_6 + 2.9360N_7 + 1.7572 \tag{8}$$

$$F_{s,UB} = 2.2006N_1 + 3.4682N_2 + 1.8026N_3 + 4.4866N_4 + 0.6495N_5 - 1.9972N_6 + 2.9439N_7 + 1.7615 \tag{9}$$

$$F_{\gamma,LB} = 2.8602N_1 + 1.4415N_2 + 10.6803N_3 + 7.9057N_4 - 4.5930N_5 - 0.6669N_6 + 2.3473N_7 + 2.1109 \tag{10}$$

$$F_{\gamma,UB} = 2.8631N_1 + 1.4243N_2 + 10.7605N_3 + 7.9666N_4 - 4.6255N_5 - 0.6506N_6 + 2.3605N_7 + 2.1130 \tag{11}$$

where:

$$N_1 = \text{tansig}\left(1.1786\phi + 0.9919\frac{H}{D} - 2.8154\right)$$

$$N_2 = \text{tansig}\left(0.3020\phi + 0.8066\frac{H}{D} - 0.7231\right)$$

$$N_3 = \text{tansig}\left(-0.7221\phi + 0.2695\frac{H}{D} + 0.8450\right)$$

$$N_4 = \text{tansig}\left(0.6964\phi - 0.0273\frac{H}{D} - 0.6421\right)$$

$$N_5 = \text{tansig}\left(-0.7325\phi + 0.4543\frac{H}{D} + 1.0060\right)$$

$$N_6 = \text{tansig}\left(0.1593\phi + 0.9393\frac{H}{D} - 0.8591\right)$$

$$N_7 = \text{tansig}\left(-0.5917\phi - 0.3726\frac{H}{D} + 0.3939\right)$$

To validate the prediction model, Fig. 9 compares the stability factors obtained from the FELA method to those predicted by the ANN model in Eqs. (6)–(11). The three subfigures represent F_c, F_s, and F_γ (LB and UB), respectively. In this Figure, the data points cluster more closely along the line $y = x$ if the values obtained from the numerical approach and ANN predictor are in agreement. It is clear that the ANN model accuracy is proven by noting all data points on the centerline. This theory is supported by an R^2 value of approximately 1.0, suggesting a high confidence level when using the seven-neuron model. Notably, this novel formula approximates the parameter values within the range provided, as previously detailed. Consequently, the results may be unreliable if the input values are outside this range.

Moreover, these proposed equations would be more persuasive if applied to input variables that did not appear in the previous set. Consequently, an additional dataset with 20 ϕ and H/D pairs, as shown in Table 9, was analyzed, and their FELA results are listed in Table 10. Thereafter, the R^2 and MSE values were obtained based on the FELA results and ANN predictions described in Fig. 10. More specifically, the ANN model showed remarkable accuracy and the ability to make predictions using the new data, as indicated by its low MSE values of 0.4420 and 0.4399 for F_c, 0.5501 and 0.5852 for F_s and 0.7949 and 0.7322 for F_γ in the UB and LB solutions, respectively. The high R^2 values in all cases (approximately 0.9998), emphasize the strong correlation between the ANN predictions and actual values. This underscores ANN model reliability and accuracy in predicting the results for an additional dataset within the training data range.

Garson's modified equation [39,40] was adopted to further assess

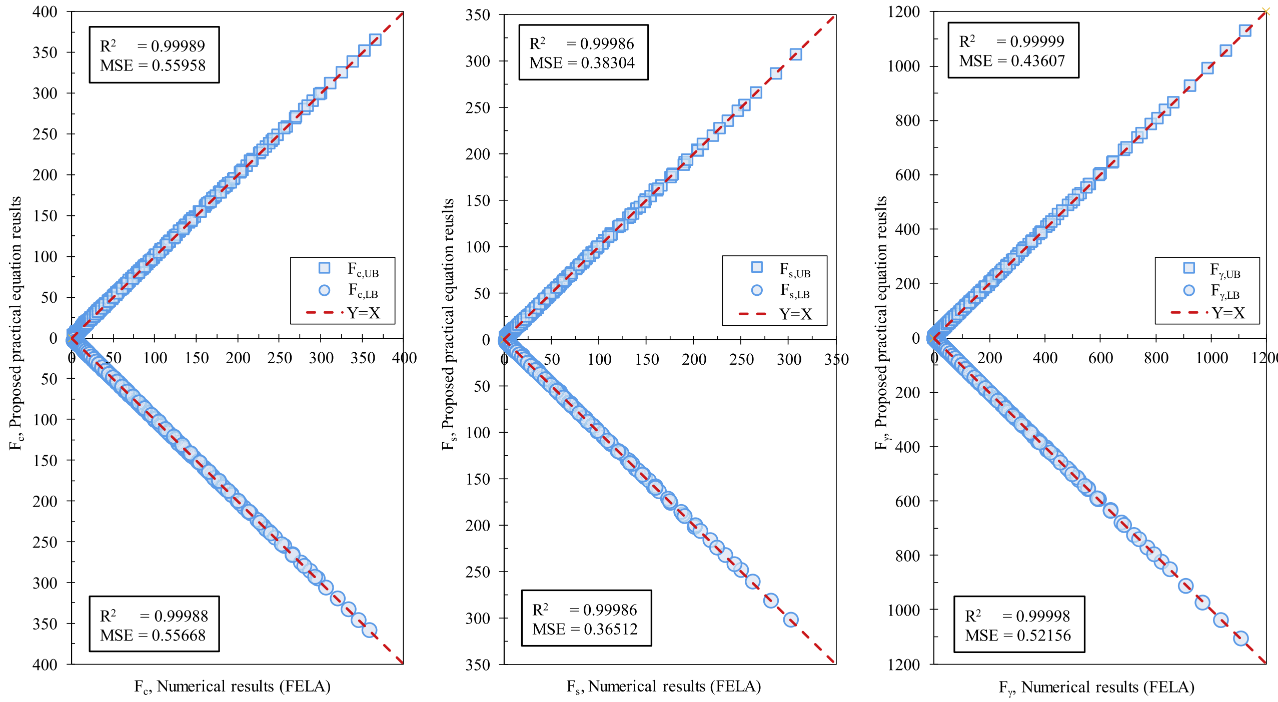

Fig. 9. Comparisons between FELA results and ANN predictions.

Table 9
The two input variable range with 20 additional cases.

Parameter	Range of values
ϕ	5.5, 15.5, 25.5, 35.5
H/D	1.5, 2.5, 5.5, 7.5, 8.5

the input parameter (ϕ and H/D) effects on the stability factors. This is shown in Eq. (12), in which the optimal model weight and bias matrices are used for the assessment.

$$I_j = \frac{\sum_{m=1}^{m=N_h}\left(\frac{|w^{ih}_{jm}|}{\sum_{k=1}^{k=N_i}|w^{ih}_{km}|} \times |w^{ho}_{mn}|\right)}{\sum_{k=1}^{k=N_i}\left[\sum_{m=1}^{m=N_h}\left(|w^{ih}_{km}| \Big/ \sum_{k=1}^{k=N_i}|w^{ih}_{km}|\right) \times |w^{ho}_{mn}|\right]} \tag{12}$$

where I_j is the j_{th} input variable relative importance, N_i and N_h are the number of input and hidden neurons, respectively, W is the connection weight, and the superscripts i, h, and o are the input, hidden, and output layers, respectively, whereas the subscripts k, m, and n are the input, hidden, and output neurons, respectively.

The weight assigned to each input variable reflects its relative importance in calculating the output value. The greater the weight, the higher the influence. The results of this study, as presented by the relative importance index, are shown in Fig. 11. The results show that ϕ

Table 10
F_c, F_s and F_γ for 20 additional cases with various depth ratios (H/D = 1.5, 2.5, 5.5, 7.5, 8.5).

ϕ	H/D	F_c, LB	F_c, UB	F_s, LB	F_s, UB	F_γ, LB	F_γ, UB
5.5	1.5	6.303	6.818	1.655	1.657	2.104	2.105
5.5	2.5	10.883	10.930	2.049	2.052	4.177	4.182
5.5	5.5	19.294	19.400	2.858	2.868	11.976	13.020
5.5	7.5	23.461	23.610	3.163	3.177	18.566	18.633
5.5	8.5	24.541	24.718	3.363	3.381	21.126	23.213
15.5	1.5	8.422	8.443	3.337	3.345	3.272	3.276
15.5	2.5	16.299	16.404	5.521	5.540	7.980	8.008
15.5	5.5	41.341	41.723	12.462	12.587	35.226	36.660
15.5	7.5	56.963	57.912	15.930	17.098	67.394	68.516
15.5	8.5	64.827	65.710	18.563	18.780	85.820	88.663
25.5	1.5	11.187	11.216	5.891	5.945	4.998	4.919
25.5	2.5	22.357	22.147	11.240	12.899	13.717	13.740
25.5	5.5	71.108	72.134	35.055	36.013	83.379	86.079
25.5	7.5	112.920	114.912	54.489	55.882	180.148	182.328
25.5	8.5	135.289	137.575	64.864	67.919	244.520	248.005
35.5	1.5	12.246	12.305	8.724	10.444	7.312	7.342
35.5	2.5	26.937	27.159	20.266	21.340	21.625	22.829
35.5	5.5	104.975	106.233	77.139	77.427	159.418	163.367
35.5	7.5	180.980	183.594	129.404	133.518	370.553	379.591
35.5	8.5	225.833	230.410	160.460	165.963	521.192	533.716

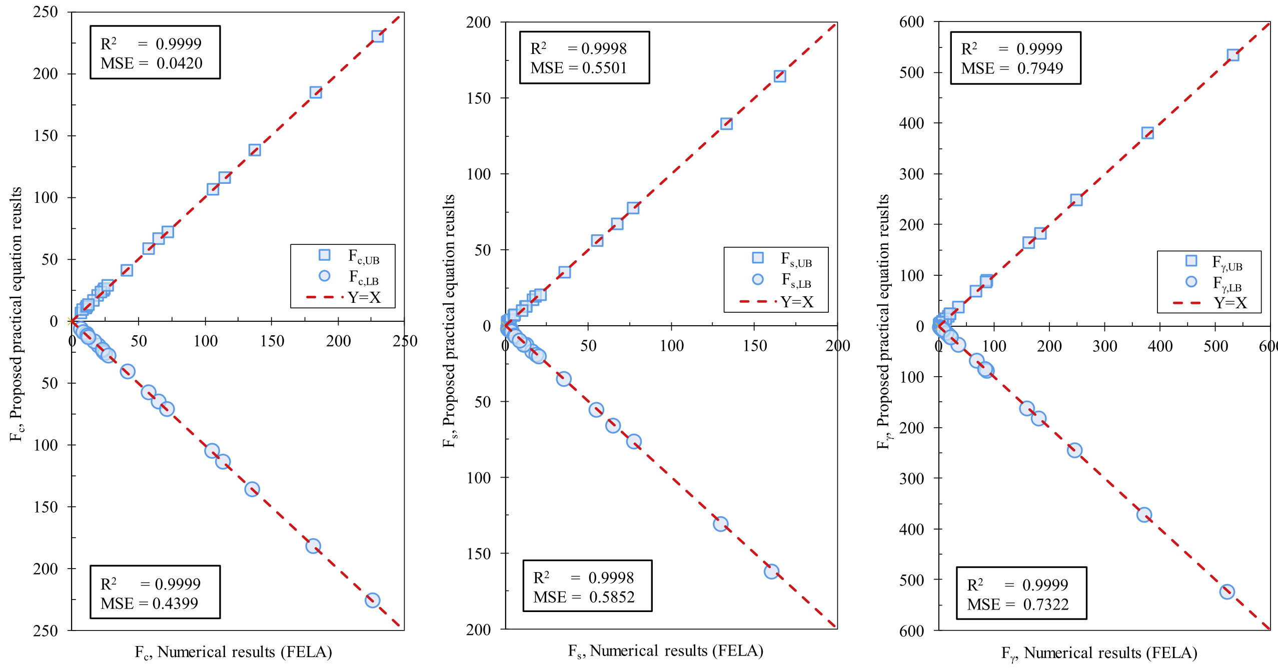

Fig. 10. Comparisons between FELA results and ANN predictions with 20 additional cases.

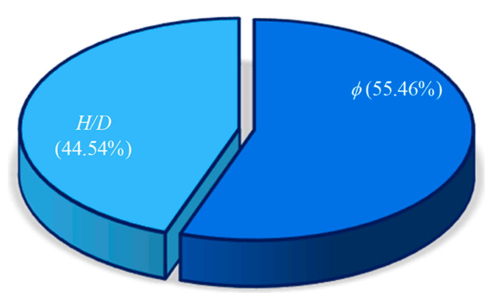

Fig. 11. The two input variables (ϕ and H/D) relative importance index.

is the most critical parameter, with a 55.46 % relative importance index, compared to 44.54 % for the H/D ratio. It is crucial that neither ϕ nor the H/D ratio should be ignored in practical analyses, because of the high importance index values.

5. Conclusion

This study successfully examined passive circular trapdoor blowout stability using axisymmetry. This problem is analogous to an underground hydrogen storage simulation under extreme blowout pressures. Three conventional stability factors were investigated using the principle of superposition and UB and LB FELA. A series of parametric results for studying the cover-depth ratio and soil internal friction angle effects were presented using design charts and tables, which can be further used to determine the critical blowout pressures under various design conditions. An example was provided to demonstrate how practical solutions can be obtained for drained passive circular trapdoors in cohesive-frictional soil.

The investigation was continued using the latest ANN approach to provide a predictive model using a large FELA result dataset. It was concluded that the optimal ANN model could provide an accurate three stability factor prediction and evaluate the critical blowout pressure final prediction given the input parameters in the investigated ranges. Therefore, this study is of practical significance to the underground engineering community.

Ethics Statement

Not applicable because this work does not involve the use of animal or human subjects.

Declaration of Competing Interest

The authors declare that they have no known competing financial interests or personal relationships that could have appeared to influence the work reported in this paper.

Data availability

The datasets used and/or analyzed in the current study are available from the corresponding author upon reasonable request.

Acknowledgment

We acknowledge Ho Chi Minh City University of Technology (HCMUT), VNU-HCM for supporting this study.

References

[1] K. Terzaghi, Stress distribution in dry and saturated sand above a yielding trapdoor, in: Proceedings, 1st International Conference on Soil Mechanics and Foundation Engineering, Cambridge, Mass, 1936.

[2] G.G. Meyerhof, J.I. Adams, The ultimate uplift capacity of foundations, Can. Geotech. J. 5 (4) (1968) 225–244.

[3] A.S. Vesic, Breakout resistance of objects embedded in ocean bottom, J. Soil Mech. Found. Div. 97 (9) (1971) 1183–1205.

[4] G.G. Meyerhof, Uplift resistance of inclined anchors and piles, in: Proc., of the 8th Int. Conf., Soil Mechanics and Foundation Engineering, Moscow 2, 1973, pp. 167–172.

[5] B.M. Das, Model tests for uplift capacity of foundations in clay, Soil Found. 18 (2) (1978) 17–24.

[6] B.M. Das, A procedure for estimation of ultimate capacity of foundations in clay, Soil Found. 20 (1) (1980) 77–82.

[7] I. Vardoulakis, B. Graf, G. Gudehus, Trap-door problem with dry sand: a statical approach based upon model test kinematics, Int. J. Numer. Anal. Meth. Geomech. 5 (1) (1981) 57–78.

[8] N.C. Koutsabeloulis, D.V. Griffiths, Numerical modelling of the trap door problem, Geotechnique 39 (1) (1989) 77–89.

[9] C.C. Smith, Limit loads for an anchor/trapdoor embedded in an associative Coulomb soil, Int. J. Numer. Anal. Meth. Geomech. 22 (11) (1998) 855–865.
[10] C.M. Martin, Undrained collapse of a shallow plane-strain trapdoor, Géotechnique 59 (10) (2009) 855–863.
[11] L. Wang, B. Leshchinsky, T.M. Evans, Y. Xie, Active and passive arching stress in C'-U' soils: a sensitivity study using computational limit analysis, Comput. Geotech. 84 (2017) 47–55.
[12] K. Terzaghi, Rock Defects and Loads on Tunnel Supports, John Wiley and Sons Inc, 1946.
[13] J. Shiau, F. Al-Asadi, Twin tunnels stability factors Fc, Fs and Fc, Geotechn. Geol. Eng. 39 (1) (2021) 335–345.
[14] J. Shiau, F. Al-Asadi, Stability factors Fc, Fs, and Fγ for twin tunnels in three dimensions, Int. J. Geomech. 22 (3) (2022), 04021290.
[15] J. Shiau, S. Keawsawasvong, Producing undrained stability factors for various tunnel shapes, Int. J. Geomech. 22 (8) (2022), 06022017.
[16] S.W. Sloan, Geotechnical stability analysis, Geotechnique 63 (7) (2013) 531–537.
[17] S.W. Sloan, Lower bound limit analysis using finite elements and linear programming, Int. J. Numer. Anal. Methods Geomech. 12 (1) (1988) 61–77.
[18] S.W. Sloan, Upper bound limit analysis using finite elements and linear programming, Int. J. Numer. Anal. Methods Geomech. 13 (3) (1989) 263–282.
[19] A.V. Lyamin, S.W. Sloan, Lower bound limit analysis using non-linear programming, Int. J. Numer. Methods Eng. 55 (5) (2002) 573–611.
[20] A.V. Lyamin, S.W. Sloan, Upper bound limit analysis using linear finite elements and non-linear programming, Int. J. Numer. Anal. Methods Geomech. 26 (2) (2002) 181–216.
[21] K. Krabbenhoft, A.V. Lyamin, S.W. Sloan, Formulation and solution of some plasticity problems as conic programs, Int. J. Solids Struct. 44 (5) (2007) 1533–1549.
[22] S. Keawsawasvong, J. Shiau, Stability of active trapdoors in axisymmetry, Undergr. Space 7 (1) (2022) 50–57.
[23] S. Keawsawasvong, J. Shiau, C. Ngamkhanong, V.Q. Lai, C. Thongchom, Undrained stability of ring foundations: axisymmetry, anisotropy, and non-homogeneity, Int. J. Geomech., ASCE 22 (1) (2022), 04021253.
[24] J. Shiau, B. Chudal, K. Mahalingasivam, S. Keawsawasvong, Pipeline burst-related ground stability in blowout condition, Transp. Geotech. 29 (2021), 100587.
[25] H. Ciria, J. Peraire, J. Bonet, Mesh adaptive computation of upper and lower bounds in limit analysis, Int. J. Numer. Methods Eng. 75 (2008) 899–944.
[26] J. Shiau, J.-S. Lee, F. Al-Asadi, Three-dimensional stability analysis of active and passive trapdoors, Tunn. Undergr. Space Technol. 107 (2021), 103635, https://doi.org/10.1016/j.tust.2020.103635.
[27] L. Wu, J. Fan, Comparison of neuron-based, kernel-based, tree-based and curve-based machine learning models for predicting daily reference evapotranspiration, PLoS One 14 (5) (2019), e0217520.
[28] M.N.A. Raja, S.K. Shukla, Multivariate adaptive regression splines model for reinforced soil foundations, Geosynth. Int. 28 (4) (2021) 368–390.
[29] D.K. Nguyen, T.P. Nguyen, C. Ngamkhanong, S. Keawsawasvong, T.K. Nguyen, V. Q. Lai, Prediction of uplift resistance of circular anchors in anisotropic clays using MLR, ANN, and MARS, Appl. Ocean Res. 136 (2023), 103584.
[30] S. Liu, R. Chang, J. Zuo, R.J. Webber, F. Xiong, N. Dong, Application of artificial neural networks in construction management: current status and future directions, Appl. Sci. 11 (20) (2021) 9616.
[31] Y. Pu, E. Mesbahi, Application of artificial neural networks to evaluation of ultimate strength of steel panels, Eng. Struct. 28 (8) (2006) 1190–1196.
[32] M. Khajehzadeh, M.R. Taha, S. Keawsawasvong, H. Mirzaei, M. Jebeli, An effective artificial intelligence approach for slope stability evaluation, IEEE Access 10 (2022) 5660–5671.
[33] D.K. Nguyen, T.P. Nguyen, C. Ngamkhanong, S. Keawsawasvong, V.Q. Lai, Bearing capacity of ring footings in anisotropic clays: FELA and ANN, Neural Comput. Appl. 35 (15) (2023) 10975–10996.
[34] S.A. Naeini, M. Khalaj, E. Izadi, Interfacial shear strength of silty sand–geogrid composite, Proc. Inst. Civ. Eng. - Geotech. Eng. 166 (1) (2013) 67–75.
[35] S.Q. Chen, J. Bai, Data-driven decision-making model for determining the number of volunteers required in typhoon disasters, J. Saf. Sci. Resil. 4 (3) (2023) 229–240.
[36] A.K. Verma, K. Kishore, S. Chatterjee, Prediction model of longwall powered support capacity using field monitored data of a longwall panel and uncertainty-based neural network, Geotech. Geol. Eng. 34 (2016) 2033–2052.
[37] F.M. Khan, R. Gupta, ARIMA and NAR based prediction model for time series analysis of COVID-19 cases in India, J. Saf. Sci. Resil. 1 (1) (2020) 12–18.
[38] F.M. Khan, A. Kumar, H. Puppala, G. Kumar, R. Gupta, Projecting the criticality of COVID-19 transmission in India using GIS and machine learning methods, J. Saf. Sci. Resil. 2 (2) (2021) 50–62.
[39] G.D. Garson, Path Analysis, Statistical Associates Publishing, Asheboro, NC, 2013.
[40] V.Q. Lai, J. Shiau, C.N. Van, H.D. Tran, S. Keawsawasvong, Bearing capacity of conical footing on anisotropic and heterogeneous clays using FEA and ANN, Mar. Georesour. Geotechnol. 41 (9) (2023) 1–18.